

Article

Wood-Biochar-Supported Magnetite Nanoparticles for Remediation of PAH-Contaminated Estuary Sediment

Cheng-Di Dong¹, Chiu-Wen Chen¹, Chih-Ming Kao², Chuan-Chi Chien³
and Chang-Mao Hung^{1,*}

¹ Department of Marine Environmental Engineering, National Kaohsiung Marine University, Kaohsiung City 81157, Taiwan; cddong@mail.nkmu.edu.tw (C.-D.D.); cwchen@mail.nkmu.edu.tw (C.-W.C.)

² Institute of Environmental Engineering, National Sun Yat-sen University, Kaohsiung City 80424, Taiwan; jkao@mail.nsysu.edu.tw

³ Industrial Technology Research Institute, Hsinchu 31057, Taiwan; varian@itri.org.tw

* Correspondence: hungcm1031@gmail.com; Tel.: +886-73-617-141 (ext. 3777); Fax: +886-73-650-548

Received: 17 January 2018; Accepted: 8 February 2018; Published: 9 February 2018

Abstract: In this study, we investigated the ability of a magnetic wood biochar (WB)-based composite catalyst (Fe₃O₄-WB) to catalyze sodium persulfate (PS) for the remediation of estuary sediment contaminated with polycyclic aromatic hydrocarbons (PAHs). The effects of various critical parameters, including the catalyst dose and initial pH, were investigated. The degradation of the PAHs was found to be related to the number of rings in their structure. The results showed that Fe₃O₄-WB is an efficient catalyst for the removal of high-ring PAHs (HPAHs), with the highest degradation rates for the 6-, 5-, and 4-ringed PAHs being 90%, 84%, and 87%, respectively, for a PS concentration of 2×10^{-5} M, catalyst concentration of 3.33 g/L, and pH of 3.0. That the reduction rate of the HPAHs was greater than that of the low-ring PAHs can be attributed to the strong affinity of the HPAHs for biochar derived from wood biomass. Overall, this study revealed that the WB-mediated electron transfer catalysis of the surface functional groups in a wide range of pH in the Fe₃O₄-WB/PS system and potentially application in the remediation of sediments contaminated with PAHs.

Keywords: biochar; wood; PAHs; sediments; remediation

1. Introduction

Sediments may contain high concentrations of persistent organic pollutants (POPs), which can have adverse effects on the environment [1,2]. Polycyclic aromatic hydrocarbons (PAHs) are among the most toxic POPs and can cause ecotoxicity in aquatic ecosystems. PAHs can be categorized into two classes: low-ring PAHs (LPAHs) (i.e., those with 2–3 rings) and high-ring PAHs (HPAHs) (i.e., those with 4–7 rings). LPAHs have been shown to exhibit significantly less toxicity as compared to HPAHs, which are ubiquitously hazardous and carcinogenic to humans [3]. Furthermore, these compounds with two or more fused aromatic rings are highly stable with respect to industrial production and human activities and are the primary PAHs found in sediments. Owing to the adverse biological effects of PAHs in aquatic ecosystems, their efficient removal from water, sediments, and soil is imperative [4].

Numerous remediation technologies have been developed to efficiently degrade and mineralize stable organic compounds present as contaminants under a broad range of conditions [5]. Using persulfate (PS) to produce strongly oxidizing sulfate radicals (SO₄^{•-}) is one of the most extensively used advanced oxidation processes (AOPs) because of its stability and high efficiency [6]. Therefore, PS oxidation may also be a suitable method for effectively treating soil contaminated with PAHs [7]. However, there exist a few limitations to using the PS oxidation technique for the treatment of contaminants. To address this issue, the electron-transfer reaction has been improved by using high-performance iron nanoparticles in the presence of SO₄^{•-} radicals in a manner similar to that of

the Fenton reaction [8]. In this process, a suitable magnetic oxide (namely, iron oxide) and its composite are used for PS oxidation to yield an effective reactive species because iron oxide is a more effective and stable catalyst as compared to soluble Fe^{2+} ions for the catalytic oxidation of organic pollutants [9–11].

Biochar is a readily available porous carbonaceous material that is produced as a solid by-product by the thermal decomposition of organic materials under oxygen-limited conditions and subsequent modification by chemical and physical methods [12]. Biochar is used widely as a soil additive, for nutrient retention in agriculture, for the adsorption of metallic and organic contaminants in sediments, as an energy generation co-product, and for mitigating climate change, because of its wide availability, low cost, and environmental friendliness [13]. A variety of biochar-based materials, such as wood-derived biochar, have received wide interest for environmental remediation applications because of their high porosity, significant quinone content, large specific surface area, large number of oxygen-containing surface functional groups, high organic carbon content, and high electron storage capacity [14,15]. Several available biochars derived from waste wood was conducted in the field of agriculture and environment application. For example, Pukalchik et al. (2017) using a combination of wood-derived biochar and humic substances can significantly improve soil quality and fertility and restore degraded soil functions, owing to the interactions between the components, resulting in the stabilization of contaminated soil [16]. The potential of magnetic wood-derived biochar for use in the treatment of metal-polluted solutions has also been investigated [17]. The results showed that biochar can significantly adsorb the heavy metal ions present in contaminated water samples, suggesting that the removal of the heavy metals is primary associated with the sorption properties of biochar. Mayakaduwa et al. (2016) achieved a maximum adsorption capacity of 44 mg/g in the case of aqueous glyphosate when using woody biochar at pH values of 5–6; the high adsorption potential could be attributed to the heterogeneous chemisorption interactions between the glyphosate and the phenolic, amine, carboxylic, and phosphate functional groups on the biochar surface [18].

Moreover, organic-waste-derived biochar can be used as a redox-active structure to promote the reductive transformation of organic compounds and thus remove redox-sensitive chemicals from the environment [19]. Zielińska and Oleszczuk (2016) studied the use of sewage-sludge-derived biochar for the immobilization of PAHs in contaminated soil [20]. The results revealed that biochar from sewage sludge rapidly immobilized the bioavailable fraction, with the effectiveness of reduction being higher in the case of soils with a lower affinity with respect to PAHs. To improve the adsorption capacity of biochar for contaminants, several methods of modifying biochar have been investigated. It has been reported that the removal of PAHs by CO_2 -activated biochar can be ascribed to the fact that biochar has a highly microporous structure (high surface area), which results in the efficient immobilization of the bioaccessible PAHs [21]. Moreover, the structures of the macropores and mesopores present in biochar allow for the adsorption of the heavier PAHs present in contaminated soil. Ouyang et al. (2017) reported magnetic biochar (Fe_3O_4 /biochar) composites for removing 1,4-dioxane from aqueous solutions [22]. They suggested that Fe_3O_4 /biochar activates PS for the degradation of 1,4-dioxane under the initial neutral pH and could achieve a removal rate of 98%. Fang et al. (2015) reported the use of biochar/PS in combination for the degradation of polychlorinated biphenyls (PCBs) [23]. They suggested that this integrated approach is highly effective for the removal of PCBs. In addition, the efficiency of rice-hull-biochar-supported nanoscale zerovalent iron (nZVI/biochar) with respect to the activation of PS for removing trichloroethylene (TCE) as the target pollutant from aqueous solutions has also been evaluated [24]. It was found that the rate of TCE degradation using the nZVI/biochar/PS technique was the highest for a reaction time of 5 min, pH of 6.2, and nZVI-to-biochar mass ratio of 1:5 in the aqueous stream. The amount of TCE degraded was high because the electron-transfer-mediating oxygen-containing functional groups of the biochar promoted the generation of $\text{SO}_4^{\cdot-}$ radicals, leading to the fast degradation of TCE.

More recently, we observed that the reduction of PAHs in marine sediment by $\text{SO}_4^{\cdot-}$ -based AOPs is enhanced by using magnetic bamboo biochar [25]. Wood biochar (WB) can help limit global warming, has fewer respiratory effects, is noncarcinogenic, and has a lower environmental impact as compared

to other types of biochars [15]. Thus, in this study, a Fe_3O_4 -WB composite was synthesized via a green method. The structure of the synthesized catalyst sample was characterized using environmental scanning electron microscopy-energy-dispersive X-ray spectrometry (ESEM-EDS), X-ray diffraction (XRD) analysis, Fourier transform infrared (FTIR) spectroscopy, and X-ray photoelectron spectroscopy (XPS). Further, the implications of the results as they relate to the potential roles of biochar-based materials in the degradation of PAHs via PS-based AOPs are discussed.

2. Results and Discussion

2.1. Characterization of Fe_3O_4 , WB, and Fe_3O_4 -WB Samples

Figure 1a shows that the Fe_3O_4 nanoparticles were spherical and exhibited a uniform particle size of approximately 50 nm. The results of the EDS analysis of the sample are shown in Figure 1. It can be seen clearly that Fe, C, and O were present in the synthesized composite. As shown in Figure 1b, the WB sample exhibited a rough, irregular, and porous structure that is typical of biochar and that Fe_3O_4 was successfully coated on the surfaces of the WB sheets Figure 1c. Further, the rough, irregular, and porous structure of WB became smoother after the deposition of Fe_3O_4 . Thus, WB can be employed for dispersing and stabilizing Fe_3O_4 in order to enhance its potential for use in environmental applications. Similar results have been reported by Mohan et al. [17] during the pyrolysis of magnetic woody biomass for the production of bio-oil.

XRD analysis was performed for 2θ values of 10 – 80° (Figure 2A). High-intensity diffraction peaks related to cubic Fe_3O_4 were observed at 30.2° , 35.5° , 43.2° , 53.5° , 57.0° , and 62.6° ; these were ascribable to the (220), (311), (400), (422), (511), and (440) planes, respectively. The sharpness of the XRD reflection peaks indicated that the Fe_3O_4 phase deposited on the surfaces of the WB sheets was highly crystalline. This probably explains why the magnetic properties as well as the face-centered cubic structure of Fe_3O_4 were maintained [9]. A peak related to amorphous graphite can be seen at 26.6° (see Figure 2A(b)) [21]. However, after the WB sample had been coated with Fe_3O_4 , a decreasing in XRD peak intensity was observed due to the Fe_3O_4 nanoparticles loading (see Figure 2A(c)); this was indicative of the Fe_3O_4 phase has been introduced into the WB of the composite catalyst. Similar type of results has been found by Wu et al. [26].

The FTIR spectra of the various materials were measured for wavelengths of 400 – 4000 cm^{-1} (Figure 2B). The samples exhibited two sharp peaks, at 445 and 640 cm^{-1} , which were related to the characteristic Fe–O stretching vibrations of the Fe_3O_4 nanoparticles. This suggested the formation of a chemical bond between the WB sheets and the Fe_3O_4 phase. It is possible that mechanical interlocking as well as coulombic interactions occurred between the Fe–O bonds on the Fe_3O_4 surface and the oxygen-containing functional groups present on the surfaces of the WB sheets [17]. A strong peak was observed at approximately 1539 cm^{-1} ; this peak was attributable to the interactions between the carboxylate (–COOH) group and the Fe_3O_4 nanoparticles. Moreover, the characteristic peak at approximately 1619 cm^{-1} corresponded to the stretching of the C=C bond in the aromatic ring. In addition, a band related to the quinoid C=O bond was observed at 1558 – 1715 cm^{-1} , while a peak related to the aliphatic chemical structure was seen at 2358 cm^{-1} [27]. Finally, the band with peaks at 1165 cm^{-1} and 1429 cm^{-1} could be ascribed to the C–O/C–O–C surface functional groups and amides (–NH₂) in the WB sample (Figure 2B(b)) [18].

The XPS survey scan of the Fe_3O_4 -WB catalyst is shown in Figure 3a, while the Fe2p, C1s, and O1s spectra are shown in Figure 3b–d. The peaks at 710.6 , 283.8 , and 531.2 eV represent the binding energies of iron, carbon, and oxygen, respectively. Further, Fe2p_{3/2} and Fe2p_{1/2} peaks were observed at 710.6 and 723.7 eV , respectively, while a C1s peak was seen at 283.8 eV . Therefore, the XPS analysis results confirmed that the Fe_3O_4 phase was firmly deposited on the WB sheets through linkages between the Fe–O–C bonds and the WB base. The BE values peak at 531.2 eV for O1s. The adsorbed oxygen diffuses rapidly to the surface vacancies and captures electrons from the conduction band of WB to form oxygen and hydroxyl anions in various forms such as O^{2-} and OH^- [28].

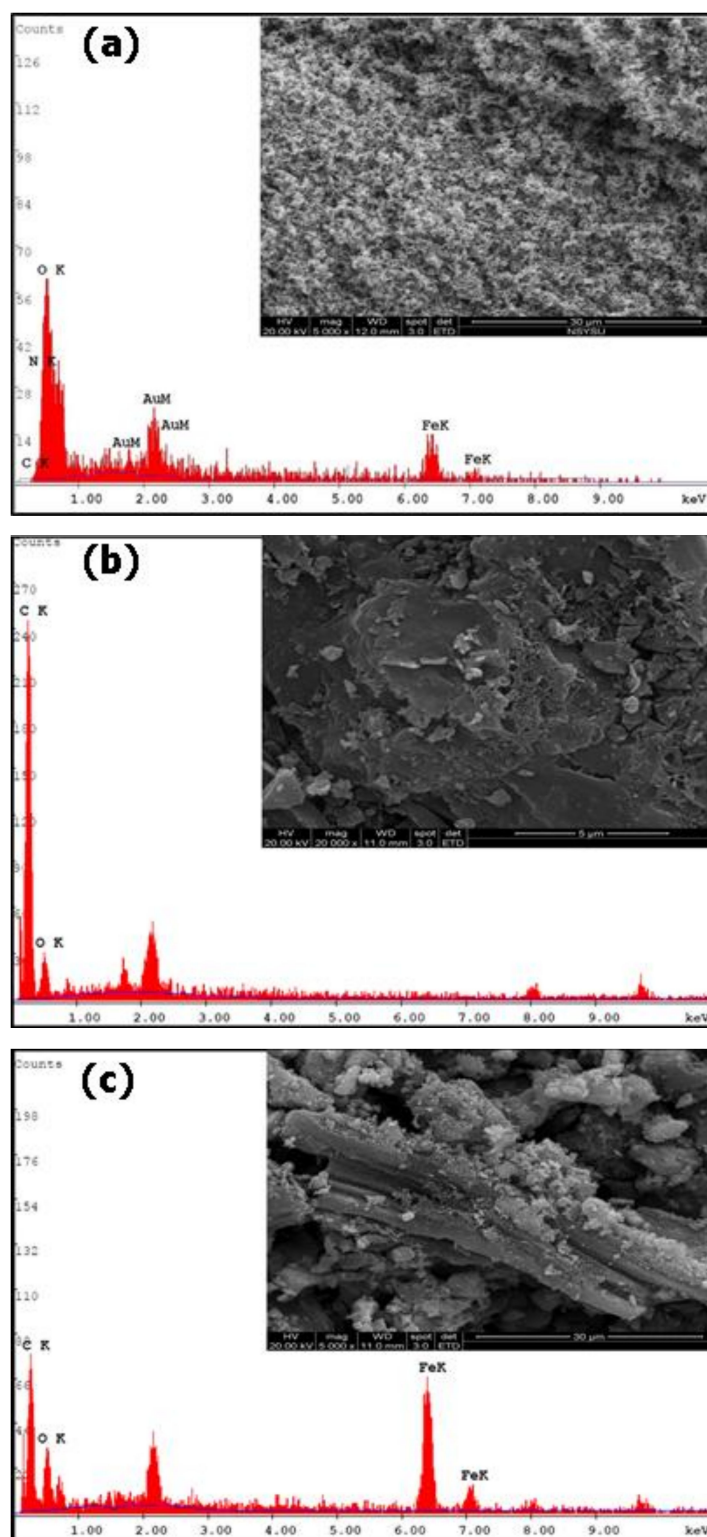


Figure 1. Environmental scanning electron microscopy–energy-dispersive X-ray spectrometry (ESEM–EDS) images of (a) Fe₃O₄, (b) wood biochar (WB), and (c) Fe₃O₄-WB.

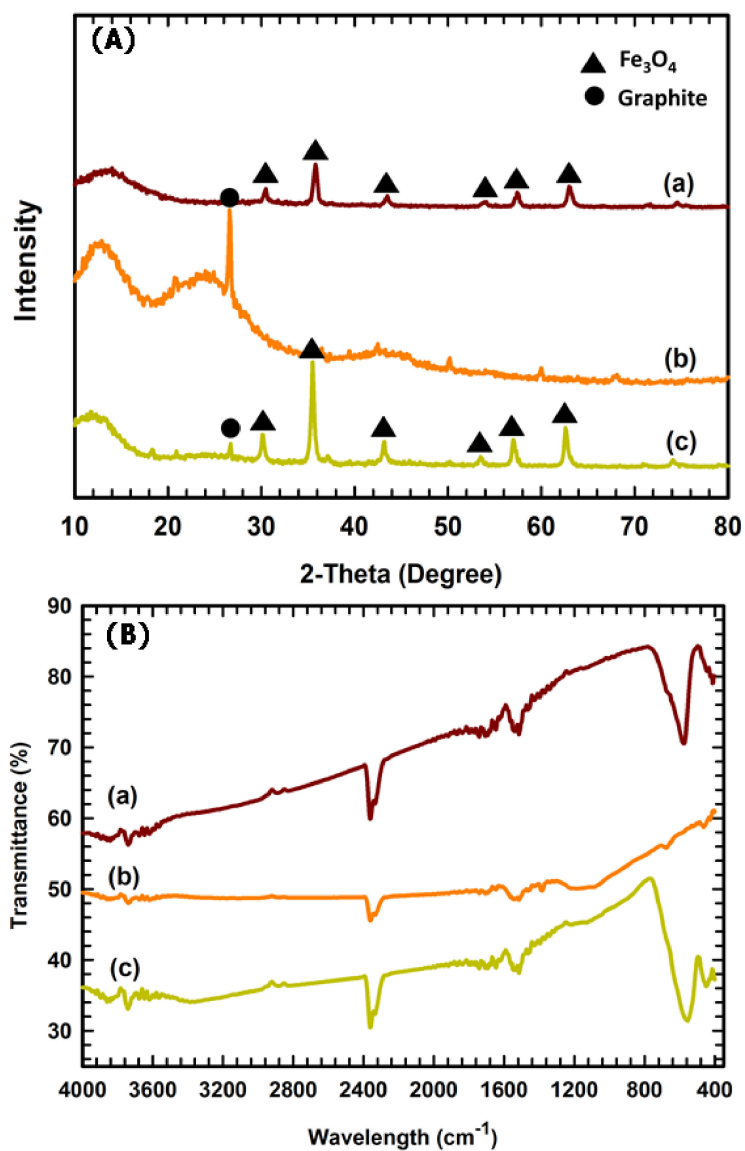


Figure 2. (A) X-ray diffraction (XRD) and (B) Fourier transform infrared (FTIR) patterns of (a) Fe₃O₄, (b) WB, and (c) Fe₃O₄-WB.

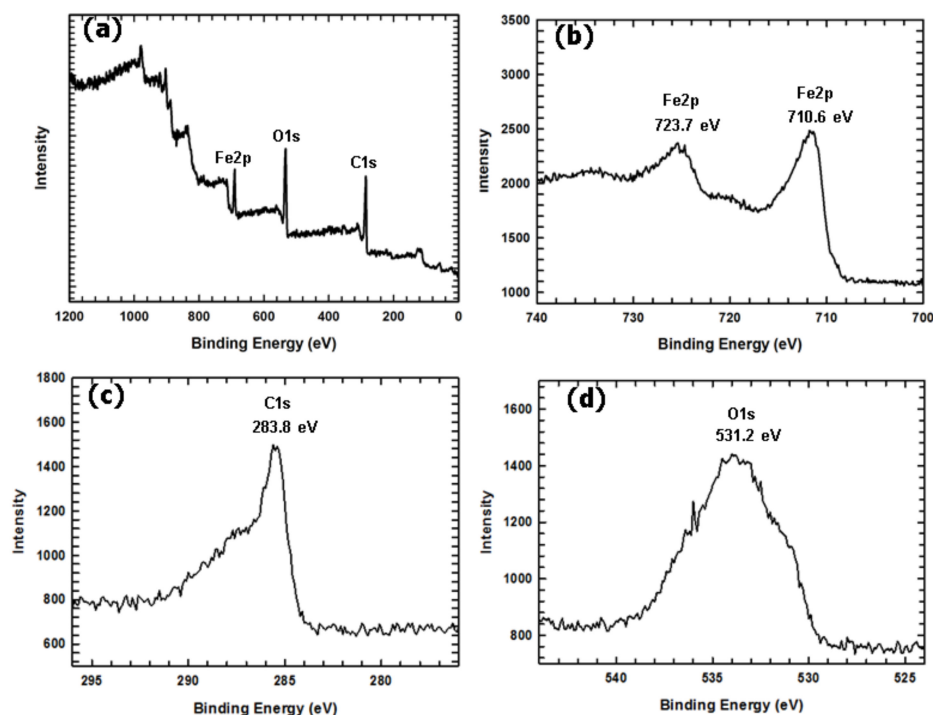


Figure 3. (a) Wide-scan X-ray photoelectron spectroscopy (XPS) spectrum and (b–d) Fe2p, C1s, and O1s core-level XPS spectra of Fe₃O₄-WB.

2.2. Catalytic Activity of Fe₃O₄-WB with Respect to PAH Reduction

The total concentration of the 16 PAHs in the untreated sediment sample was approximately 9985 ± 142 ng/g. In the sediment, naphthalene (NA), phenanthrene (PH), and pyrene (PY) were the primary PAH pollutants, with the 2-ring PAHs (NA) accounting for most of the total PAH content (22%). Figure 4a shows the effects of PS, Fe₃O₄-WB, and Fe₃O₄-WB/PS on the PAH degradation efficiency during the SO₄^{•-}-based AOP. It can be that a Fe₃O₄-WB concentration of 3.33 g/L was suitable for the effective degradation of the PAHs, with the maximum conversion rates for the PS, Fe₃O₄-WB, and Fe₃O₄-WB/PS processes being 14%, 13%, and 76%, respectively. This result confirmed that, in the absence of Fe₃O₄-WB, the direct degradation of the PAHs by PS was relatively slow and took more than 24 h. On the other hand, the Fe₃O₄-WB catalyst could activate PS to a high degree. Moreover, the decrease in the PAH content was related to the number of aromatic rings of the PAHs as well as the strong binding of the PAHs by the biochar [8]. The Fe₃O₄-WB/PS process resulted in maximum degradation rates of 74%, 75%, and 84% for the 6-ring, 5-ring, and 4-ring PAHs, respectively (Figure 4b). This suggested that the presence of WB-promoted the capacity of the biochar to reversibly donate and accept electrons within the system, thus accelerating the formation of Fe²⁺ ions and hence the generation of SO₄²⁻ ions. The mechanism by which the Fe₃O₄-WB composite activates PS is based on their surface reaction potential and the large number of oxygen-containing functional groups present on the surface of the composite. This leads to the production of Fe²⁺ ions, which act as electron-transfer mediators and initiate a reaction to generate SO₄^{•-} radicals through the Haber-Weiss mechanism [16,29]. Moreover, the thermal conversion of biomass to obtain biochar increases the porosity and aromatic surface and results in the biochar having a high negative surface charge as well as a high charge density. This also enhances the suitability of biochar for use in environmental remediation. WB containing the quinone group may undergo reversible redox reactions. This explains the catalytic ability of biochar [14]. Previous studies have suggested that C=C bonds are transformed into quinone, which activates PS during the reaction [21]. Catalytic testing showed that treatment with the Fe₃O₄-WB composite for 24 h resulted in PS exhibiting the highest activity with respect to the HPAHs. This suggests that the Fe₃O₄-WB composite, which consisted of biochar with

a macro/mesoporous structure, was suitable for adsorbing the HPAHs present in the investigated sediment [19]. Thus, it can be concluded that $S_2O_8^{2-}$ and Fe_3O_4 -WB have a synergistic effect on the degradation of PAHs.

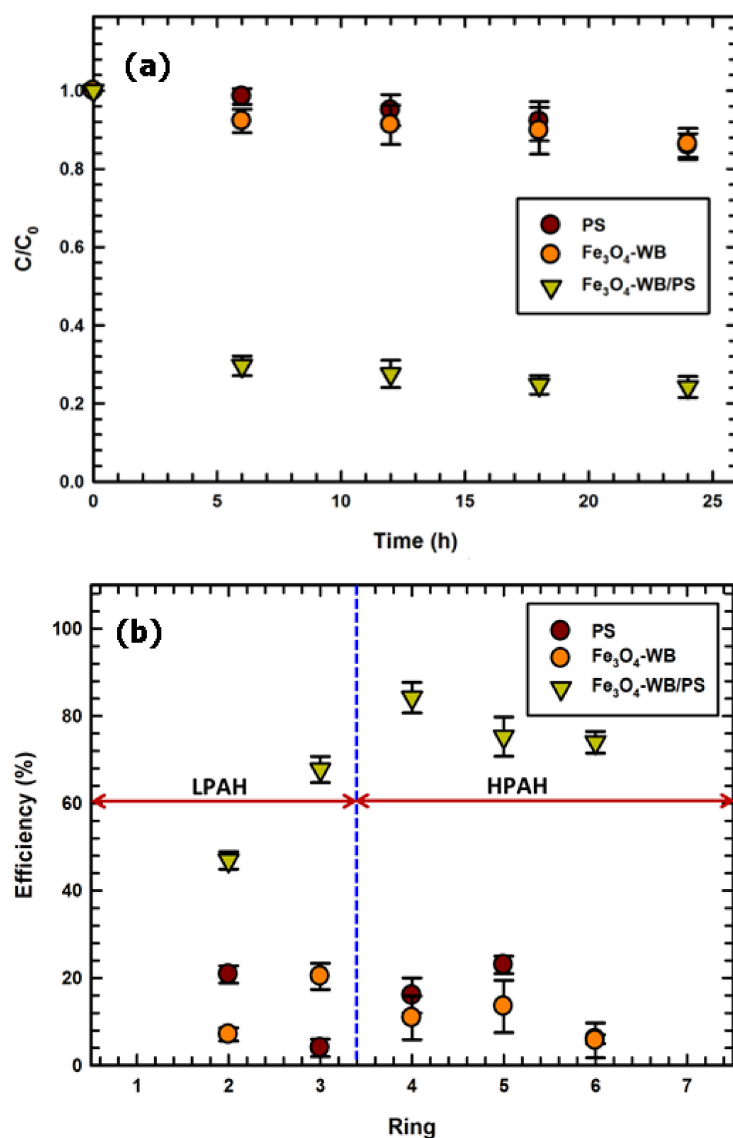


Figure 4. (a) Plots of decrease in polycyclic aromatic hydrocarbons (PAH) concentration (C/C_0) versus time and (b) efficiency of PAH degradation as function of ring number during different processes. Experimental conditions: amount of sediment = 1.00 g, reaction volume = 40 mL, $T = 303$ K, $pH_0 = 6.0$, $[Na_2S_2O_8] = 2 \times 10^{-5}$ M, $[Fe_3O_4-WB] = 3.33$ g/L, and molar ratio of PS: Σ PAHs = 1:1. LPAH: low-ring PAH; HPAH: high-ring PAH; PS: sodium persulfate.

Figure 5 shows that the degradation of the PAHs increased sharply with an increase in the concentration of Fe_3O_4 -WB from 1.67 to 6.67 g/L. At a Fe_3O_4 -WB dose of 6.67 g/L, the maximum conversion rate was 76% (Figure 5a), with the highest degradation rate for the 6-ring, 5-ring, and 4-ring PAHs being 74%, 75%, and 84%, respectively (Figure 5b). This can probably be ascribed to the increase in the catalyst dose accelerating the decomposition of PS into $SO_4^{\cdot-}$ radicals because of the presence of the Fe^{2+}/Fe^{3+} species in a sufficient high amount and the interaction of with the π -electron-rich WB surface via π - π electron donor-acceptor interactions [18,30]. The Fe^{2+} - Fe^{3+} with electron transfer catalysis by quinone-hydroquinone moieties and conjugated π -electron systems

associated with condensed aromatic redox-active structures of the WB, promoting the generation of $\text{SO}_4^{\cdot-}$ radicals in the $\text{Fe}_3\text{O}_4\text{-WB/PS}$ system [19,24]. Based on the results described above, it can be concluded that WB is a good conductor and that electrons from Fe_3O_4 are conducted through the $\text{Fe}_3\text{O}_4\text{-WB}$ composite to the PAHs such that the Fe^{2+} ions produced lead to the generation of $\text{SO}_4^{\cdot-}$ radicals. This accounts for the increase in the degradation rate of the PAHs in the case of the $\text{Fe}_3\text{O}_4\text{-WB/PS}$ system.

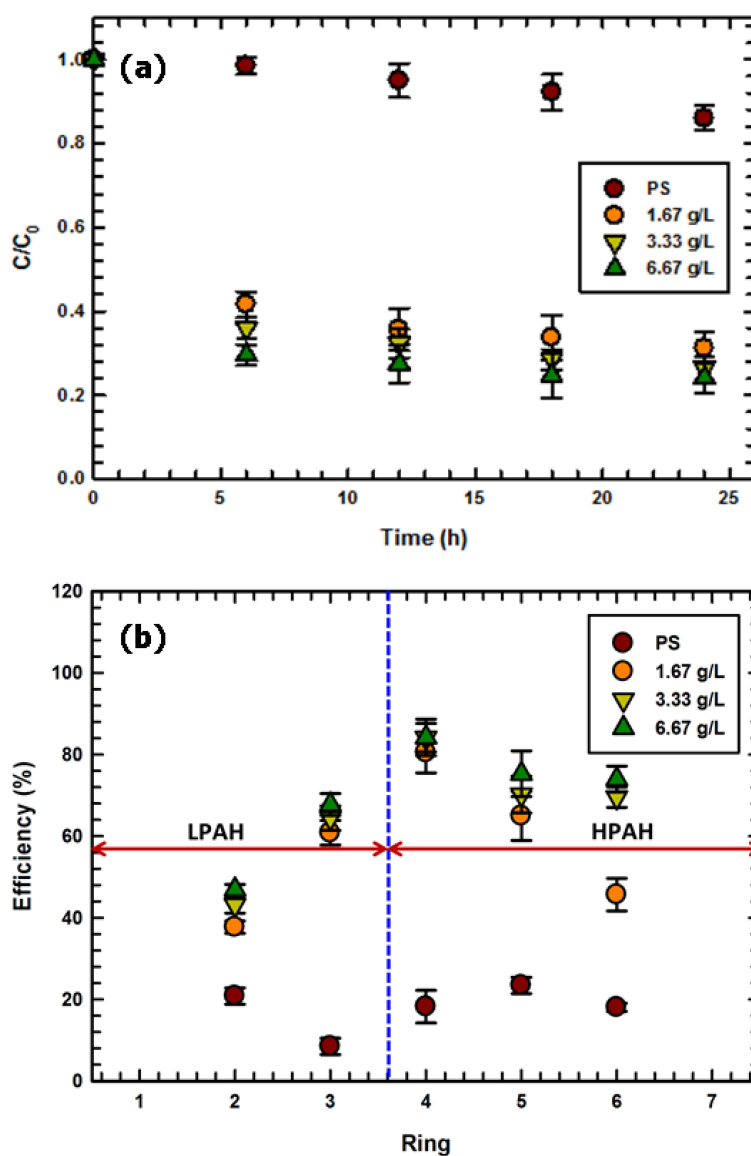


Figure 5. (a) Effect of $\text{Fe}_3\text{O}_4\text{-WB}$ catalyst dosage and (b) efficiency of PAH degradation as function of ring number for various $\text{Fe}_3\text{O}_4\text{-WB}$ catalyst dosages. Experimental conditions: amount of sediment = 1.00 g, reaction volume = 40 mL, $T = 303$ K, $\text{pH}_0 = 6.0$, $[\text{Na}_2\text{S}_2\text{O}_8] = 2 \times 10^{-5}$ M, and molar ratio of PS: $\Sigma\text{PAHs} = 1:1$.

The degradation of the PAHs using the $\text{Fe}_3\text{O}_4\text{-WB/PS}$ system was studied at pH values of 3.0–9.0. Figure 6a shows the effect of the pH on the degradation of the PAHs when $\text{Fe}_3\text{O}_4\text{-WB}$ was used as the catalyst. It can be seen that a lower pH_0 aided PAH degradation by $\text{Fe}_3\text{O}_4\text{-WB}$ (Figure 6b), whereas the degradation rate of the PAHs decreased to 76% at pH_0 6.0. The optimal pH for the degradation of the PAHs was determined to 3.0, with the highest degradation rates for the 6-ring, 5-ring, and 4-ring HPAHs being of 90%, 84%, and 87%, respectively (Figure 6b). These observations

are in keeping with those reported by Perez-Gregorio et al. [31], who stated that HPAHs are reduced to a greater degree by wood ash than are LPAHs by organic solvents because of the strong affinity of the HPAHs for biochar. It is known that $\text{SO}_4^{\bullet-}$ is the dominant active free radical in aqueous acidic phases. Thus, the pH of the system has a marked effect on the activity of PS, as $\text{SO}_4^{\bullet-}$ is the main active species at lower pH levels and has a greater oxidizing capacity than that of $\bullet\text{OH}$ [32]. Therefore, more $\text{SO}_4^{\bullet-}$ radicals are generated by the Fe^{2+} ions through the activation of PS. This explains why an acidic environment is favorable for the removal of PAHs by the $\text{Fe}_3\text{O}_4\text{-WB/PS}$ process. Furthermore, the solution pH has a determining effect on the degradation of PAHs because it influences the protonation of the functional groups on the biochar surface. Biochar containing electroactive quinoid functional groups and polycondensed aromatic sheets can act as an electron shuttle to mediate electron-transfer reactions [19,23]. Within this context, several mechanisms can occur on the biochar surface, including redox reactions and donor-acceptor complex formation, with many of these mechanisms being pH dependent [33]. Furthermore, with respect to the sorption properties of biochar, it has been shown that biochar has a strong affinity for PAHs [20,30]. Consequently, the $\text{Fe}_3\text{O}_4\text{-WB}$ concentration should be controlled such that the adverse effects of $\text{Fe}_3\text{O}_4\text{-WB}$ on $\text{SO}_4^{\bullet-}$ production are minimized. The results of this study indicated that the $\text{Fe}_3\text{O}_4\text{-WB/PS}$ process is a stable and efficient one over a wide pH range (3.0–9.0).

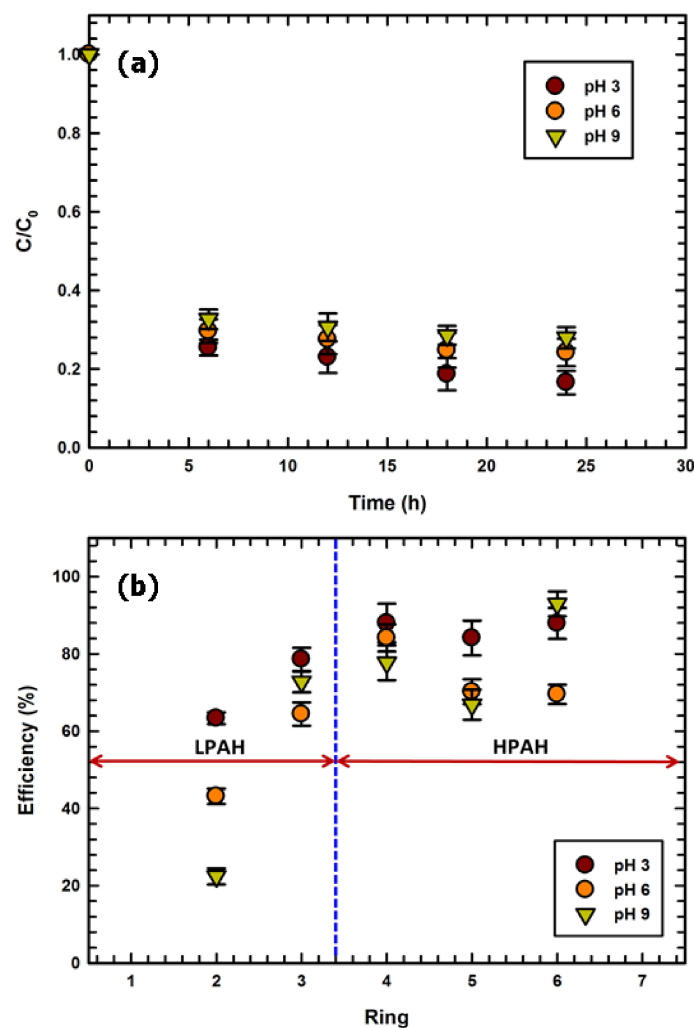


Figure 6. (a) Effect of initial pH and (b) efficiency of PAH degradation as function of ring number for various initial pH levels. Experimental conditions: amount of sediment = 1.00 g, reaction volume = 40 mL, $T = 303\text{ K}$, $[\text{Na}_2\text{S}_2\text{O}_8] = 2 \times 10^{-5}\text{ M}$, $[\text{Fe}_3\text{O}_4\text{-WB}] = 3.33\text{ g/L}$, and molar ratio of PS: $\Sigma\text{PAHs} = 1:1$.

3. Materials and Methods

3.1. Materials and Chemicals

3.1.1. Sediment Samples

The PAH-contaminated sediment used in this study was collected with an Ekman Dredge Grab from a depth of approximately 20 cm from the industrialized estuaries of Kaohsiung City, Taiwan. This area is characterized by sediment contaminated with multiple contaminants, which are produced by smelting activities. After collection, the sediment samples were freeze-dried for 72 h before being homogenized with a sieve (0.5 mm), macerated, and placed in previously cleaned glass bottles for further analysis.

3.1.2. Chemicals Used

The following chemicals were purchased from Merck: acetone, methanol, and n-hexane (99.8%, HPLC grade). $\text{Na}_2\text{S}_2\text{O}_8$ (PS) (98%) was purchased from Showa Chemical Industry Co. (Tokyo, Japan). Standards of 16 PAHs in an 80 mg/L mixture solution, deuterated PAH internal standard solutions at a concentration of 4000 mg/L, and surrogate standard solutions at 2000 mg/L were obtained from AccuStandard Chem. Co. (New Haven, CT, USA). All the other reagents used were of analytical grade. Deionized water was used throughout the study for solution preparation.

The WB (Industrial Technology Research Institute, Hsinchu, Taiwan) sample was prepared from dried pellets of Lauan wood chips via pyrolysis at 573 K in a flow of purified N_2 using a pilot-scale plant. The WB sample was washed thoroughly, oven-dried at 333 K for 24 h, and then crushed with a grinder and sieved to ensure a particle size of 2.5 mm. The specific surface area of the WB sample was $40 \text{ m}^2/\text{g}$, as determined by the Brunauer–Emmett–Teller method using N_2 . The method used for synthesizing the Fe_3O_4 nanoparticles is described in detail elsewhere [10]. The magnetically responsive Fe_3O_4 –WB catalyst was synthesized using a co-precipitation approach. In brief, before Fe_3O_4 deposition, 10 g of the WB substrate was dispersed in a HCl solution. The substrate was then filtered, washed with ethanol several times, and vacuum dried for 24 h. Subsequently, the Fe_3O_4 –WB composite with 10 wt % Fe_3O_4 was dispersed in the WB matrix. After the WB sheets had been coated with Fe_3O_4 , the mixture was stirred continuously and dispersed by ultrasonication for 30 min. The obtained product was calcinated at 573 K in a N_2 stream for 6 h. Finally, the resulting composite was cooled at room temperature and washed with distilled water to remove any unreacted chemicals. The thus-produced composite was used for the remainder of the experiment.

3.2. Experimental Methods

The experiments were performed using 40-mL borosilicate amber bottles containing 1 g of the sediment and 25 mL of an oxidizer as vial reactors. The oxidizer and the PAHs were added in a 1:1 ratio. All the bottles were placed in a horizontal position on a platform shaker (SB-9D, Taiwan Hipoint Corporation, Kaohsiung City, Taiwan) rotating at 200 rpm. The temperature of the reaction mixture was controlled automatically at 298 K. Finally, at the end of each experiment, KI was added to quench the oxidizer degradation reactions for obtaining the representative PAH concentrations. As mentioned previously, 16 PAHs (Naphthalene (NA), Acenaphthylene (ACY), Acenaphthene (ACE), Fluorene (FL), Phenanthrene (PH), Anthracene (AN), Fluoranthene (FLU), Pyrene (PY), Benz[a]anthracene (BaA), Chrysene (CH), Benzo[b]fluoranthene (BbF), Benzo[k]fluoranthene (BkF), Benzo[a]pyrene (BaP), Indeno[1,2,3-cd]pyrene (IP), Dibenzo[a,h]anthracene (DA) and Benzo[ghi]perylene (BP)) classified by the United States Environmental Protection Agency as being high priority for environmental monitoring were analyzed. All experiments were performed in triplicate and the mean and standard deviations are reported.

3.3. Instrumental Analyses

The determination and quantification of PAHs in sediment samples were determined using a gas chromatography/mass spectrometry (GC/MS) system (Model 6890/5975, Agilent Technologies, Santa Clara, CA, USA), in order to account for all the PAHs in the test sample. The conditions for the analysis of the PAHs have been described in detail previously [25]. The surface morphology of the catalyst was determined using an ESEM system equipped with an EDS attachment (Quanta 200 FEG, FEI Company, Brno-Černovice, Czech Republic). XRD analysis was performed using a Diano-8536 diffractometer (Siemens, Karlsruhe, Germany) equipped with a Cu-K α radiation source. The FTIR spectrum of the catalyst was recorded on an FTIR spectrometer (FT-700, Horiba, Kyoto, Japan). The crystal structure and chemical composition of the catalyst were investigated using XPS (AXIS Ultra DLD, Kratos Analytical Ltd., Manchester, UK).

4. Conclusions

In this study, we demonstrated that Fe₃O₄ particles synthesized by the co-precipitation method and incorporated into wood biomass can be used for the effective remediation of sediment contaminated with high-ring PAHs through chemical oxidation. The oxidation of the PAHs was related to the number of rings in their structure. It was found that the Fe₃O₄-WB composite served as an activator for the accelerated formation of SO₄^{-•} radicals during the PS oxidation reaction and reduced the content of HPAHs in the sediment sample in the following order: 6-ring > 4-ring > 5-ring PAHs. Therefore, the Fe₃O₄-WB composite is an efficient remediation material for removing PAHs from contaminated sediment.

Acknowledgments: The authors would like to thank the Ministry of Science and Technology of the Republic of China, Taiwan, for financially supporting this study under Contract Nos. MOST 106-2221-E-022-002-MY3 and 106-2221-E-022-003-MY3.

Author Contributions: Cheng-Di Dong conceived and designed the experiments; Chiu-Wen Chen performed the experiments; Chang-Mao Hung analyzed the data; Chih-Ming Kao and Chuan-Chi Chien contributed the reagents/materials/analysis tools; and Chang-Mao Hung wrote the paper.

Conflicts of Interest: The authors declare no conflict of interest.

References

1. Cardoso, F.D.; Dauner, A.L.L.; Martins, C.C. A critical and comparative appraisal of polycyclic aromatic hydrocarbons in sediments and suspended particulate material from a large South American subtropical estuary. *Environ. Pollut.* **2016**, *214*, 219–229. [[CrossRef](#)] [[PubMed](#)]
2. Pintado-Herrera, M.G.; Wang, C.; Lu, J.; Chang, Y.P.; Chen, W.; Li, X.; Lara-Martín, P.A. Distribution, mass inventories, and ecological risk assessment of legacy and emerging contaminants in sediments from the Pearl River Estuary in China. *J. Hazard. Mater.* **2017**, *323*, 128–138. [[CrossRef](#)] [[PubMed](#)]
3. Kuppusamy, S.; Thavamani, P.; Venkateswarlu, K.; Lee, Y.B.; Naidu, R.; Megharaj, M. Remediation approaches for polycyclic aromatic hydrocarbons (PAHs) contaminated soils: Technological constraints, emerging trends and future directions. *Chemosphere* **2017**, *168*, 944–968. [[CrossRef](#)] [[PubMed](#)]
4. Gong, C.; Shen, G.; Huang, H.; He, P.; Zhang, Z.; Ma, B. Removal and transformation of polycyclic aromatic hydrocarbons during electrocoagulation treatment of an industrial wastewater. *Chemosphere* **2017**, *168*, 58–64. [[CrossRef](#)] [[PubMed](#)]
5. Waclawek, S.; Lutze, H.V.; Grübel, K.; Padil, V.V.T.; Černík, M.; Dionysiou, D.D. Chemistry of persulfates in water and wastewater treatment: A review. *Chem. Eng. J.* **2017**, *330*, 44–62. [[CrossRef](#)]
6. Hung, C.M.; Chen, C.W.; Liu, Y.Y.; Dong, C.D. Decolorization of methylene blue by persulfate activated with FeO magnetic particles. *Water Environ. Res.* **2016**, *88*, 675–686. [[CrossRef](#)] [[PubMed](#)]
7. Zhao, D.; Liao, X.; Yan, X.; Huling, S.G.; Chai, T.; Tao, H. Effect and mechanism of persulfate activated by different methods for PAHs removal in soil. *J. Hazard. Mater.* **2013**, *254–255*, 228–235. [[CrossRef](#)] [[PubMed](#)]

8. Oleszczuk, P.; Kołtowski, M. Effect of co-application of nano-zero valent iron and biochar on the total and freely dissolved polycyclic aromatic hydrocarbons removal and toxicity of contaminated soils. *Chemosphere* **2017**, *168*, 1467–1476. [[CrossRef](#)] [[PubMed](#)]
9. Jung, K.W.; Choi, B.H.; Jeong, T.U.; Ahn, K.H. Facile synthesis of magnetic biochar/Fe₃O₄ nanocomposites using electro-magnetization technique and its application on the removal of acid orange 7 from aqueous media. *Bioresour. Technol.* **2016**, *220*, 672–676. [[CrossRef](#)] [[PubMed](#)]
10. Hung, C.M.; Chen, C.W.; Jhuang, Y.J.; Dong, C.D. Fe₃O₄ magnetic nanoparticles: Characterization and performance exemplified by the degradation of methylene blue in the presence of persulfate. *J. Adv. Oxid. Technol.* **2016**, *19*, 43–51. [[CrossRef](#)]
11. Su, C. Environmental implications and applications of engineered nanoscale magnetite and its hybrid nanocomposites: A review of recent literature. *J. Hazard. Mater.* **2017**, *322*, 48–84. [[CrossRef](#)] [[PubMed](#)]
12. Oh, S.Y.; Son, J.G.; Chiu, P.C. Biochar-mediated reductive transformation on nitro herbicides and explosives. *Environ. Toxicol. Chem.* **2013**, *32*, 501–508. [[CrossRef](#)] [[PubMed](#)]
13. Ye, L.; Zhang, J.; Zhao, J.; Luo, Z.; Tu, S.; Yin, Y. Properties of biochar obtained from pyrolysis of bamboo shoot shell. *J. Anal. Appl. Pyrolysis* **2015**, *114*, 172–178. [[CrossRef](#)]
14. Saquing, J.M.; Yu, Y.H.; Chiu, P.C. Wood-derived black carbon (biochar) as a microbial electron donor and acceptor. *Environ. Sci. Technol.* **2016**, *3*, 62–66. [[CrossRef](#)]
15. Thompson, K.A.; Shimabuku, K.K.; Kearns, J.P.; Knappe, D.R.U.; Summers, R.S.; Cook, S.M. Environmental comparison of biochar and activated carbon for tertiary wastewater treatment. *Environ. Sci. Technol.* **2016**, *50*, 11253–11262. [[CrossRef](#)] [[PubMed](#)]
16. Pukalchik, M.; Mercl, F.; Panova, M.; Břendová, K.; Terekhova, V.A.; Tlustoš, P. The improvement of multi-contaminated sandy loam soil chemical and biological properties by the biochar, wood ash, and humic substances amendments. *Sci. Total Environ.* **2017**, *229*, 516–524. [[CrossRef](#)] [[PubMed](#)]
17. Mohan, D.; Kumar, H.; Sarswat, A.; Alexandre-Franco, M.; Pittman, C.U. Cadmium and lead remediation using magnetic oak wood and oak bark fast pyrolysis bio-chars. *Chem. Eng. J.* **2014**, *236*, 513–528. [[CrossRef](#)]
18. Mayakaduwa, S.S.; Kumarathilaka, P.; Herath, I.; Ahmad, M.; Al-Wabel, M.; Ok, Y.S.; Usman, A.; Abduljabbar, A.; Vithanage, M. Equilibrium and kinetic mechanisms of woody biochar on aqueous glyphosate removal. *Chemosphere* **2016**, *144*, 2516–2521. [[CrossRef](#)] [[PubMed](#)]
19. Klüpfel, L.; Keiluweit, M.; Kleber, M.; Sander, M. Redox properties of plant biomass-derived black carbon (Biochar). *Environ. Sci. Technol.* **2014**, *48*, 5601–5611. [[CrossRef](#)] [[PubMed](#)]
20. Zielińska, A.; Oleszczuk, P. Bioavailability and bioaccessibility of polycyclic aromatic hydrocarbons (PAHs) in historically contaminated soils after lab incubation with sewage sludge-derived biochars. *Chemosphere* **2016**, *163*, 480–489. [[CrossRef](#)] [[PubMed](#)]
21. Kołtowski, M.; Hilber, I.; Bucheli, T.D.; Charmas, B.; Skubiszewska-Zięba, J.; Oleszczuk, P. Activated biochars reduce the exposure of polycyclic aromatic hydrocarbons in industrially contaminated soils. *Chem. Eng. J.* **2017**, *310*, 33–40. [[CrossRef](#)]
22. Ouyang, D.; Yan, J.; Qian, L.; Chen, Y.; Han, L.; Su, A.; Zhang, W.; Ni, H.; Chen, M. Degradation of 1,4-dioxane by biochar supported nano magnetite particles activating persulfate. *Chemosphere* **2017**, *184*, 609–617. [[CrossRef](#)] [[PubMed](#)]
23. Fang, G.; Liu, C.; Gao, J.; Dionysiou, D.D.; Zhou, D. Manipulation of persistent free radicals in biochar to activate persulfate for contaminant degradation. *Environ. Sci. Technol.* **2015**, *49*, 5645–5653. [[CrossRef](#)] [[PubMed](#)]
24. Yan, J.; Han, L.; Gao, W.; Xue, S.; Chen, M. Biochar supported nanoscale zerovalent iron composite used as persulfate activator for removing trichloroethylene. *Bioresour. Technol.* **2015**, *175*, 269–274. [[CrossRef](#)] [[PubMed](#)]
25. Dong, C.D.; Chen, C.W.; Hung, C.M. Synthesis of magnetic biochar from bamboo biomass to activate persulfate for the removal of polycyclic aromatic hydrocarbons in marine sediments. *Bioresour. Technol.* **2017**, *245*, 188–195. [[CrossRef](#)] [[PubMed](#)]
26. Wu, H.; Feng, Q.; Yang, H.; Alam, E.; Gao, B.; Gu, D. Modified biochar supported Ag/Fe nanoparticles used for removal of cephalexin in solution: Characterization, kinetics and mechanisms. *Colloids Surf. A Physicochem. Eng. Asp.* **2017**, *517*, 63–71. [[CrossRef](#)]
27. Xu, T.; Lou, L.; Luo, L.; Cao, R.; Duan, D.; Chen, Y. Effect of bamboo biochar on pentachlorophenol leachability and bioavailability in agricultural soil. *Sci. Total Environ.* **2012**, *414*, 727–731. [[CrossRef](#)] [[PubMed](#)]

28. Miyakoshi, A.; Ueno, A.; Ichikawa, M. XPS and TPD characterization of manganese-substituted iron–potassium oxide catalysts which are selective for dehydrogenation of ethylbenzene into styrene. *Appl. Catal. A Gen.* **2001**, *219*, 249–258. [[CrossRef](#)]
29. Li, H.; Wan, J.; Ma, Y.; Wang, Y. Synthesis of novel core-shell $\text{Fe}_0@Fe_3O_4$ as heterogeneous activator of persulfate for oxidation of dibutyl phthalate under neutral conditions. *Chem. Eng. J.* **2016**, *301*, 315–324. [[CrossRef](#)]
30. Sun, K.; Kang, M.; Zhang, Z.; Jin, J.; Wang, Z.; Pan, Z.; Xu, D.; Wu, F.; Xing, B. Impact of deashing treatment on biochar structural properties and potential sorption mechanisms of phenanthrene. *Environ. Sci. Technol.* **2013**, *47*, 11473–11481. [[CrossRef](#)] [[PubMed](#)]
31. Perez-Gregorio, M.R.; García-Falcón, M.S.; Martínez-Cerballo, E.; Simal-Gándara, J. Removal of polycyclic aromatic hydrocarbons from organic solvents by ashes wastes. *J. Hazard. Mater.* **2010**, *178*, 273–281. [[CrossRef](#)] [[PubMed](#)]
32. Ma, Z.; Yang, Y.; Jiang, Y.; Xi, B.; Yang, T.; Peng, X.; Lian, X.; Yan, K.; Liu, H. Enhanced degradation of 2,4-dinitrotoluene in groundwater by persulfate activated using iron–carbon micro-electrolysis. *Chem. Eng. J.* **2017**, *311*, 183–190. [[CrossRef](#)]
33. Karunanayake, A.G.; Dewage, N.B.; Todd, O.A.; Essandoh, M.; Anderson, R.; Mlsna, T.; Mlsna, D. Salicylic acid and 4-nitroaniline removal from water using magnetic biochar: An environmental and analytical experiment for the undergraduate laboratory. *J. Chem. Educ.* **2016**, *93*, 1935–1938. [[CrossRef](#)]



© 2018 by the authors. Licensee MDPI, Basel, Switzerland. This article is an open access article distributed under the terms and conditions of the Creative Commons Attribution (CC BY) license (<http://creativecommons.org/licenses/by/4.0/>).